Reaction temperature variations on the crystallographic state of spinel cobalt aluminate

ARTICLE *in* DALTON TRANSACTIONS · MARCH 2013

Impact Factor: 4.2 · DOI: 10.1039/c3dt32828g · Source: PubMed

10 AUTHORS, INCLUDING:

Minori Taguchi
Chuo University
27 PUBLICATIONS **531** CITATIONS
SEE PROFILE

Yoshio Sakka
National Institute for Materials Science
718 PUBLICATIONS **7,624** CITATIONS
SEE PROFILE

Hiroya Abe
Osaka University
154 PUBLICATIONS **1,113** CITATIONS
SEE PROFILE

Takashi Naka
National Institute for Materials Science
129 PUBLICATIONS **1,373** CITATIONS
SEE PROFILE

Dalton Transactions

RSC Publishing

PAPER

Reaction temperature variations on the crystallographic state of spinel cobalt aluminate†

Cite this: *Dalton Trans.*, 2013, **42**, 7167

Minori Taguchi,*[a,b] Takayuki Nakane,[b] Kenjiro Hashi,[b] Shinobu Ohki,[b] Tadashi Shimizu,[b] Yoshio Sakka,[b] Akiyuki Matsushita,[b] Hiroya Abe,[c] Toshitaka Funazukuri[a] and Takashi Naka[b]

Received 27th November 2012,
Accepted 5th March 2013

DOI: 10.1039/c3dt32828g

www.rsc.org/dalton

In this study, we report a rapid and simple technique for obtaining cobalt aluminate having a spinel structure. The products were prepared from a hydroxide precursor synthesized by coprecipitation of cobalt (Co^{2+}) and aluminum (Al^{3+}) nitrates with an alkaline solution. The chosen precursor enabled low temperature fabrication of cobalt aluminate with a spinel structure by sintering it for 2 hours at low temperatures (>400 °C). Crystallographic and thermal analyses suggest that the low-temperature-sintered products contain Co^{3+} ions stabilized by chemisorbed water and/or hydroxide groups, which was not observed for products sintered at temperatures higher than 1000 °C. The color of the products turned from clear blue (Thenard's blue) to dark green when sintering temperatures were below 1000 °C. Magnetic quantities, Curie constants, and Weiss temperatures show a strong dependence on the sintering temperature. These findings suggest that there are mixed valent states, *i.e.* Co^{2+} and Co^{3+}, and unique cation distributions at the different crystallographic sites in the spinel structure, especially in the products sintered at lower temperatures.

Introduction

Spinel-type transition metal oxides have attracted much attention in the inorganic chemistry, solid-state physics, and materials science fields because of their interesting magnetic, optical, electronic, and catalytic properties.[1–3] The (normal) spinel structure is represented as AB_2O_4, where the A and B sites indicate di- and trivalent metal cations, respectively, of two different tetrahedral (T_d) and octahedral (O_h) sites in the structure.[1–3] Among spinel materials, cobalt aluminate ($CoAl_2O_4$), known as Thenard's blue pigment, is widely used in the ceramic industry as a coloring agent in glazes and porcelain stoneware because of its thermal and chemical stability.[4–6] Recently, $CoAl_2O_4$ has also been found to be an effective catalyst in methane reformation[7] and may be a useful catalyst in the photoelectrochemical splitting of H_2O.[8–10] The magnetic properties are interesting because it is a magnetic spin system with frustrated exchange interactions.[11–15] Additionally, the physical properties of $CoAl_2O_4$ depend on the crystallographic parameters, such as the lattice constant, the crystallite size, and the cation distribution,[16–18] and therefore tuning it will be expected to result in not only improvement of the properties but also discovery of novel properties.

To synthesize $CoAl_2O_4$, the conventional solid-phase reaction (sintering) method of binary oxides of CoO (or Co_3O_4) and α-Al_2O_3 is generally employed. This process, however, requires a high reaction temperature (>1000 °C) and a long reaction time.[11–15] Sol–gel methods have become an important preparation technique,[18–24] and although these methods enable preparation of $CoAl_2O_4$ nanoparticles, complicated procedures, such as sequential addition of reagents, are required to precisely control the sol–gel conditions. Resultingly, the sol–gel precursors were heat-treated at temperatures above 400 °C for obtaining spinel $CoAl_2O_4$ crystals.

Recently, we have developed a technique for the simple and rapid synthesis of metal oxides and corresponding nanoparticles through a hydrothermal method employing hydroxide precursors.[25–32] The method can be used for the preparation of not only simple metal oxides, but also surface-modified metal oxides. In fact, $CoAl_2O_4$ nanoparticles have also been synthesized by this method using a Co–Al hydroxide as the precursor,[31] showing that the use of the hydroxide precursor can lead to rapid crystallization of $CoAl_2O_4$ under low temperature (<400 °C) conditions. Although the nanoparticles almost had single phase of a spinel structure, the molar ratio of Al/Co ions was about 5 and lattice defects were present in the crystal structure.[32] Since the amount of the Co ion that resulted in the

[a]*Department of Applied Chemistry, Faculty of Science and Engineering, Chuo University, 1-13-27 Kasuga, Bunkyo-ku, Tokyo 112-8551, Japan. E-mail: mtaguchi@chuo-u.ac.jp*
[b]*National Institute for Materials Science, 1-2-1 Sengen, Tsukuba 305-0047, Japan*
[c]*Joining and Welding Research Institute, Osaka University, 11-1 Mihogaoka, Ibaraki, Osaka 567-0047, Japan*

†Electronic supplementary information (ESI) available: A photograph and ^{27}Al-NMR spectra of the products are shown, as are the χ–T plots of the products and Co_3O_4 synthesized from $Co(OH)_2$. See DOI: 10.1039/c3dt32828g

blue color[19–24] was small, the color of the nanoparticles was indeed dilute blue.[31] The non-stoichiometry in the $CoAl_2O_4$ nanoparticles seemed to be caused by the different solubility of the metal (Co and Al) ions under the hydrothermal condition. The different solubility might affect the crystallization process for spinel-type $CoAl_2O_4$. These results suggest that the control of the stoichiometry, especially in the case of synthesis of ternary metal oxide products like $CoAl_2O_4$, is very difficult under the hydrothermal condition. Control of the solubility of the metal ions on adding other reagents is necessary in order to prepare the products with tuning the stoichiometry by using hydrothermal methods. In contrast, the solid-phase reaction (sintering) method can precisely control the stoichiometry of the metal ions in the products. Additionally, the hydrothermal method is not suitable for synthesis above ~500 °C. However the Co–Al hydroxide precursor utilized by the hydrothermal method is indeed effective for rapid crystallization and lower temperature preparation of $CoAl_2O_4$.

Consequently, we focused on a hydroxide precursor utilized by the hydrothermal method and the conventional sintering method of maintaining a stoichiometry ratio. By sintering a Co–Al hydroxide precursor, uniform $CoAl_2O_4$ products while maintaining the stoichiometry of the metal ions can be synthesized at low temperature. By controlling the preparation temperature, tunability of the lattice constant and the crystallite size of spinel-type $CoAl_2O_4$ can be achieved. As will be shown herein, the heating temperature strongly affects the crystallographic, optical, and magnetic characteristics of the spinel $CoAl_2O_4$ products. Therefore, in this study, we have systematically synthesized spinel $CoAl_2O_4$ products *via* sintering of a hydroxide precursor at various temperatures and evaluated the properties of the products with respect to the structural, optical, and magnetic characteristics.

Experimental

Sample preparation

The starting materials of $Co(NO_3)_2{\cdot}6H_2O$, $Al(NO_3)_3{\cdot}9H_2O$, and NaOH were purchased from Wako Chemicals. The Co–Al hydroxide precursor material was prepared by coprecipitation with an alkaline solution. The two metal nitrates were dissolved in distilled water (100 ml) at room temperature with a molar ratio of Al^{3+}/Co^{2+} = 2.00 and a total concentration of 0.10 M. In another container, NaOH was dissolved in distilled water (100 ml) at a concentration of 0.30 M. The NaOH solution was slowly added to the solution of metal nitrates. This process yielded a pink slurry, which was stirred at room temperature for 24 hours in order to allow the reaction to take place. After 24 hours, the unreacted material was removed through a combination of repeated and alternating centrifugation and decantation with distilled water several times. Finally, the obtained pink product, the hydroxide precursor, was dried in a vacuum for 24 hours. The hydroxide precursor was sintered in a furnace at a selected temperature (from 400 to 1400 °C in increments of 200 °C) for 2 hours in a covered alumina crucible under an air atmosphere. The heating rate to the target temperature was fixed at 10 °C min^{-1}. Hereafter, the products obtained from the precursor are denoted as **400** (sintering at 400 °C), **600** (at 600 °C), **800** (at 800 °C), **1000** (at 1000 °C), **1200** (at 1200 °C), and **1400** (at 1400 °C).

Reference compounds, $Co(OH)_2$ and $Al(OH)_3$, were prepared separately from $Co(NO_3)_2{\cdot}6H_2O$ and $Al(NO_3)_3{\cdot}9H_2O$, respectively, by precipitation with NaOH solution.

Characterization methods

Elemental analysis of the sintered products was monitored for Al and Co by an inductively coupled plasma atomic emission spectrometer (ICP-AES) and was conducted by Sumitomo Metal Technology, Inc. The molar ratio of Al to Co in the precursor was almost the same (2.05 ± 0.01) for all of the products.

X-ray diffraction (XRD) patterns of the products were recorded using a RINT-2500 diffractometer (Rigaku) with Cu Kα (λ = 1.5416 Å) radiation at a 2θ scan speed of 2° min^{-1}. The lattice constant was calculated from the XRD patterns of the products using a unit cell parameter refinement program (Cell Calc).[33] The Scherrer equation was used to determine the crystallite size of the spinel structure products from the full width at half maximum (FWHM) of the typical peaks (220, 311, 400, 422, 511, and 440) and using a shape factor of 0.9. Additionally, structural (lattice) defects of the products were verified through analysis of the typical peaks in a Williamson–Hall plot.[34] Note that the FWHM of the typical peaks as W (vertical axis) was used in this plot instead of the integral width of the peaks. For reference, the XRD pattern of normal spinel $CoAl_2O_4$ was simulated using CrystalMaker and CrystalDiffract software (CrystalMaker Software Ltd). The parameters used in the simulation were: X-ray wavelength (λ) = 1.5416 Å, crystallite size = 100 nm, and lattice constant = 8.106 Å.

To analyze the crystal structure of the **800** product, a synchrotron XRD (SXRD) measurement for it was carried out at NIMS beamline BL15XU, SPring-8. A large Debye–Scherrer camera and an imaging plate were used along with monochromatic synchrotron radiation with wavelength 0.65297 Å, which was measured from the X-ray absorption edge of niobium, and CeO_2 was selected as a standard material of SXRD measurements. The fine powdered sample was packed into a Lindenmann-glass capillary of 0.1 mm in diameter. The SXRD data were recorded in a 2θ range of 3–60° at a step interval of 0.003°. The linear absorption coefficient of each sample was estimated by measurement of the transmittance of the incident X-ray beam. The diffraction pattern was refined by the Rietveld method using the RIETAN-FP program. In the refinement process, the crystallographic parameters of the **800** product (*e.g.* unit cell parameters, atomic positions, cationic distribution, and isotropic temperature factors) were refined, and we also considered an impurity γ-alumina with a spinel structure[35] and estimated the molar ratio of Al to Co from the ICP-AES.

Thermogravimetric and differential thermal analyses (TG–DTA) of the precursor were performed using a DTG-60H (Shimadzu) from room temperature to 1500 °C at a ramping rate of 10 °C min^{-1} without flowing gas. Fourier transform

infrared (FT-IR) spectra were recorded using an FT/IR-6200 spectrometer (JASCO) with KBr pellets. UV–VIS powder diffuse reflectance spectra were recorded using a V-650 spectrometer (JASCO). The obtained spectra were converted to absorption spectra using the Kubelka–Munk calculation.[26] The coloration of the products was numerically evaluated with the $L^*a^*b^*$ color parameters, which were calculated by the CIE $L^*a^*b^*$ colorimetric method (JIS Z8701-1999) with standard lighting C and a view angle of 10°.

The magnetic properties of the products were evaluated using a superconducting quantum interference device magnetometer (SQUID, MPMS-XL, Quantum Design). The temperature dependencies of the magnetic susceptibilities, χ, and inverse susceptibilities, χ^{-1}, at a magnetic field of 100 Oe (after zero-field-cooled (ZFC) and field-cooled (FC)) were measured for the temperature, T, in the range from 2.0 to 300 K. The Weiss temperature, θ, and the Curie constant, C, were determined from the experimental data of the χ^{-1}–T curves between 50 and 300 K using the Curie–Weiss law, $\chi = C/(T - \theta)$. The effective moment, p_{eff}, was calculated using the equation $p_{\mathrm{eff}} = (3k_{\mathrm{B}}/N_{\mathrm{A}}\mu_{\mathrm{B}} \times C)^{1/2}$, where k_{B}, N_{A}, and μ_{B} are the Boltzmann constant, Avogadro's number, and the Bohr magneton, respectively. The theoretical effective moment ($p_{\mathrm{eff\text{-}theo}}$) of normal spinel $CoAl_2O_4$ was calculated using the equation $p_{\mathrm{eff\text{-}theo}} = g \times (S(S + 1))^{1/2}$, where g is the g-factor and S is the spin quantum number of the Co^{2+} ion at the T_{d} site in the spinel structure. The g-factor value was assumed to be 2.4.[15] The spin quantum number, S, of the Co^{2+} ion was 3/2 at the T_{d} site.[16] As for normal spinel $CoAl_2O_4$, there is no coexistence of Co ions at the O_{h} site. We verified the consistency of the magnetic susceptibility for the **800** product. Based on the result of Rietveld refinement, the $p_{\mathrm{eff\text{-}cal}}$ of the product was calculated using the equation $p_{\mathrm{eff\text{-}cal}} = [nl(p_{\mathrm{eff}}T_{\mathrm{d}})^2 + 2nm(p_{\mathrm{eff}}O_{\mathrm{h}})^2]^{1/2}$, where l and m are the abundance ratios of the Co^{2+} ion at the T_{d} and O_{h} sites, respectively, $p_{\mathrm{eff}}T_{\mathrm{d}}$ is the $p_{\mathrm{eff\text{-}cal}}$ of the Co^{2+} ion with a high spin state at the T_{d} site, and $p_{\mathrm{eff}}O_{\mathrm{h}}$ is the $p_{\mathrm{eff\text{-}cal}}$ of the Co^{2+} ion with a high spin state at the O_{h} site. n is the molar ratio of the spinel cobalt aluminate content in the **800** product, which is estimated to be 0.56.

Solid-state NMR spectra of ^{27}Al (I = 5/2, $\gamma/2\pi$ = 11.094 MHz T^{-1}) were recorded in a magnetic field of 9.4 T at room temperature for the wide-band regions. Because some NMR spectra were too broad to be uniformly excited with a single pulse, the wide-band NMR spectra were obtained by summing a set of FT spectra and shifting the transient frequency at an interval of 100 kHz. Each of the FT spectra was obtained by performing a Fourier transform on a half of a spin echo signal excited with a π/2 pulse of 2 μs and a π pulse of 4 μs.

Results and discussion

1. Properties of the precursor

XRD patterns of $Co(OH)_2$ and $Al(OH)_3$ (Fig. 1) were consistent with JCPDS cards (74-1057 and 83-2256, respectively). In addition to the peaks from $Al(OH)_3$, the XRD pattern of the precursor (Fig. 1) showed pronounced peaks around 2θ = 23 and 35°. These peaks were assigned to a Co–Al hydrotalcite (Co–AlHtc) structure,[36] showing that the precursor was composed of $Al(OH)_3$ and Co–AlHtc. Peaks from $Co(OH)_2$ were not found in the pattern for the precursor.

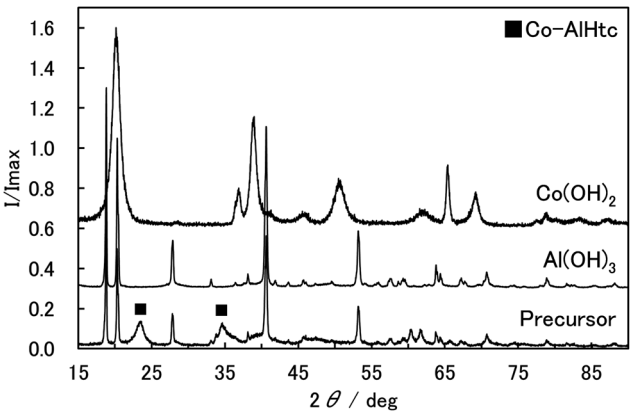

Fig. 1 XRD patterns of $Co(OH)_2$, $Al(OH)_3$, and the precursor. (■) The peaks were assigned to a Co–AlHtc structure.

To study the thermal stability of the precursor, TG–DTA measurements were performed (Fig. 2). For $Co(OH)_2$ (Fig. 2a), around 300 and 900 °C, significant weight loss and related changes in the endothermicity were observed. The former phenomenon was assigned to the decomposition and/or the melting of $Co(OH)_2$, and the latter was assigned to the reduction of Co_3O_4 to CoO.[37,38] The oxidation from Co^{2+} to Co^{3+} became apparent around 200 °C,[37] and the reduction from Co^{3+} to Co^{2+} occurred around 900 °C. For $Al(OH)_3$ (Fig. 2b), distinctive weight loss and a related endothermic peak were seen around 300 °C in the TGA and DTA curves, respectively. They were assigned to the decomposition and/or the melting of $Al(OH)_3$.[39] For the precursor (Fig. 2c), the main weight loss was below 300 °C, and the TGA curve looked similar to that of $Al(OH)_3$. The DTA curve of the precursor, however, differed from both the $Co(OH)_2$ and $Al(OH)_3$ curves in that there were three distinct endothermic peaks at 220, 250, and 300 °C. The peaks at 220 and 250 °C were attributed to the release of interlayer water and the intercalated anions in the Co–AlHTc, respectively.[36] The peak at 300 °C was assigned to the decomposition and/or the melting of the Co–AlHTc and $Al(OH)_3$.[36,39] The weight loss of the precursor occurred gradually over a broad range of temperature between 300 and 800 °C and may possibly be the result of pyrolytic elimination of residual hydroxide groups.[21] These results suggest that the precursor does not completely decompose and/or melt below 300 °C. Additionally, a subtle change was detected around 950 °C in the DTA curve of the precursor. This suggests the presence of a small amount of Co^{3+} ions below 1000 °C, and the reduction from Co^{3+} to Co^{2+} ions between 900 and 1000 °C. However, the amount of pure Co_3O_4 as a residual product seems to be quite small in this sample, and the distinctive weight loss around 950 °C was not observed in the DTA curve for $Co(OH)_2$ (Fig. 2a).

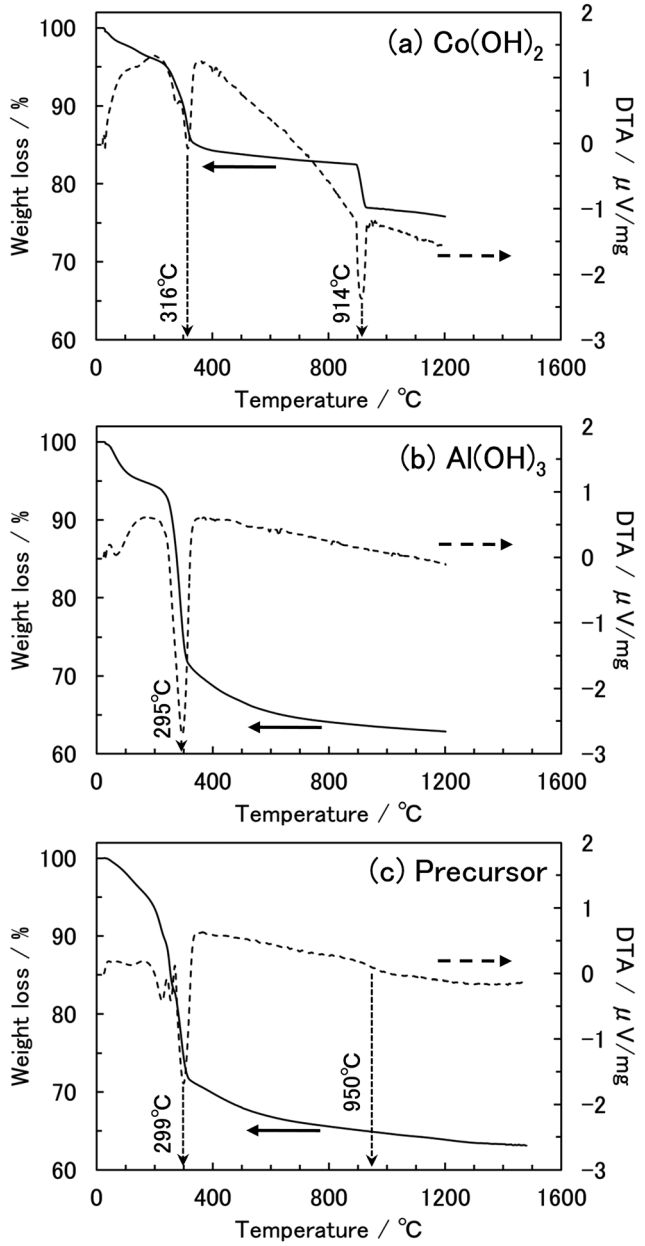

Fig. 2 TG (solid lines) and DTA (dashed lines) curves for (a) $Co(OH)_2$, (b) $Al(OH)_3$, and (c) the precursor. The measurements were conducted at a temperature ramp rate of 10 °C min^{-1} without flowing gas.

2. XRD analysis of the products

Typical sintering temperatures for the solid–solid reaction of $CoAl_2O_4$ to achieve a blue color are generally known to be over 1000 °C.[12–15] Products with a blue color were also obtained in this study at temperatures above 1000 °C, denoted by **1000–1400** (see Fig. S1†). However, the colors of the **400–800** products were dark green. The XRD patterns of the **1000–1400** products (Fig. 3) were clearly that of a spinel structure assigned to face-centered-cubic (space group $Fd\bar{3}m$) $CoAl_2O_4$. This is consistent with the other studies.[4–24] Interestingly, XRD patterns for the **400–800** products (Fig. 3) could be also assigned as having a spinel structure. Although the peak widths in the

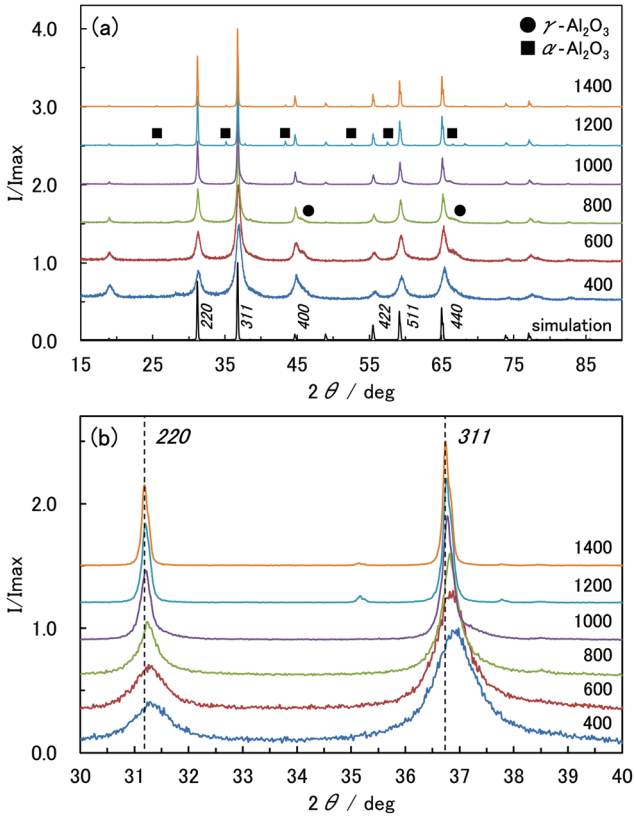

Fig. 3 XRD patterns of the products (a) sintered at temperatures between 400 and 1400 °C and (the bottom pattern) the simulated XRD pattern of $CoAl_2O_4$ and (b) the evolution of the characteristic 220 and 311 reflections. The peaks were assigned to (●) γ-Al_2O_3 (spinel structure) and (■) α-Al_2O_3 (corundum structure).

XRD patterns of the **400–800** products were broader than those of the **1000–1400** products, they seem to have the same spinel structure. Note that the signal of a spinel structure was also found in the product sintered at 200 °C, although $Al(OH)_3$ peaks were still present. This result is consistent with the TG–DTA result, which showed that the main reaction of the precursor starts to occur around 200 °C. Therefore, the critical process in the formation of all of the products, regardless of the final color of the product, seems to be the synthesis of a spinel cobalt aluminate above 200 °C. Pérez-Ramírez *et al.* investigated the thermal decomposition of a Co–Al hydrotalcite (HTc) product (Co/Al = 3) in air.[36] It decomposed above 150 °C and crystallized as a spinel metal oxide (a solid solution of Co_3O_4, Co_2AlO_4, and $CoAl_2O_4$ denoted as $Co(Co,Al)_2O_4$) above 200 °C. This spinel structure was enhanced with increasing heating temperature. The decomposition and crystallization of the HTc product are similar to those of our precursor in this study. So, low-temperature fabrication of spinel cobalt aluminate products can be successfully executed using a hydroxide precursor and the preparation process outlined herein. It should be pointed out that while the main component represented in the XRD of the products is cobalt aluminate having a spinel structure (Fig. 3a), additional weak peaks and structures in the patterns were identified and assigned to

γ-Al_2O_3 (spinel structure) and α-Al_2O_3 (corundum structure). The phase transition from γ- to α-Al_2O_3 occurred around 1000 °C.[40]

Changes in the XRD peaks at 220 and 311 with sintering temperature systematically shifted to high angle with decreasing temperature (Fig. 3b), suggesting the reduction of the lattice constants of the products. Peaks for the **400–800** products were broader than those of the **1000–1400** products. The lattice constants and crystallite sizes of the products were clearly smaller for the products formed at lower temperature (Table 1). The lattice constants of the **1000–1400** products were close to those of stoichiometric $CoAl_2O_4$.[13–18,24] The peak shift of the XRD pattern is likely caused by local distortions in the lattice and/or the cation distribution. In fact, previous reports have shown that the randomness of the cation distribution and the degree of lattice defects can influence the lattice constant.[16–18] In order to evaluate the lattice defects in the products, an indexed Williamson–Hall plot[34] was created using the crystallite sizes determined from the Scherrer equation (Fig. 4). The gradients in the plot for the **1000–1400** products were small. In fact, these plots can be approximated as a flat line, suggesting that local distortions are small. Additionally, deviations from the line at the respective indices imply that the lattice defects are isotropic. In contrast, positive gradients in the plots for the **400–800** products are very clear, even though the deviations from the linear square line are large. This suggests that there are anisotropic local distortions in the **400–800** products. Sintering temperature variations, therefore, have a significant impact on the crystallite size, lattice constants, and the degree of local distortion due to defects and/or cation distribution in the spinel-type cobalt aluminate. Tsunekawa *et al.* investigated the dependence of the crystallite size on the lattice constant for the metal oxide nanoparticles, showing that the lattice constants of nanoparticles tended to increase with decreasing crystallite size.[41] This is caused by the lattice defects such as oxygen vacancies. That is, lattice defects are easy to produce in nanosized crystals. The increase of lattice constants was indeed seen in our previous studies for metal oxide nanoparticles.[25–30] Therefore, the crystallite size possibly correlates with the degree of lattice defects. This evaluation suggested a transition for the crystallinity between 800 and 1000 °C, which is possibly due to the reduction from Co^{3+} to Co^{2+} ions and the phase transition from γ- to α-Al_2O_3 around 1000 °C. From the viewpoint of the crystallinity, low-temperature products (400 to 800 °C) are distinguished from high-temperature products (1000 to 1400 °C).

Based on the results, the XRD pattern of the **800** product measured by a synchrotron source was evaluated using the Rietveld refinement (Fig. 5). The lattice constants, a, the oxygen positional parameters, x_O, molar ratio, site occupancies, g, isotropic thermal factors, B_{iso}, and Bragg reliability parameters, R_B, for the respective phases in the product (cobalt (Co) and aluminum (Al) cations on the tetrahedral (T_d or A-) and octahedral (O_h or B-) sites) are listed in Table 2. The composition of the **800** product was estimated at $(Co_{0.87}Al_{0.13})[Al_{0.60}Co_{0.40}]_2O_4$, where (...) and [...] represent the

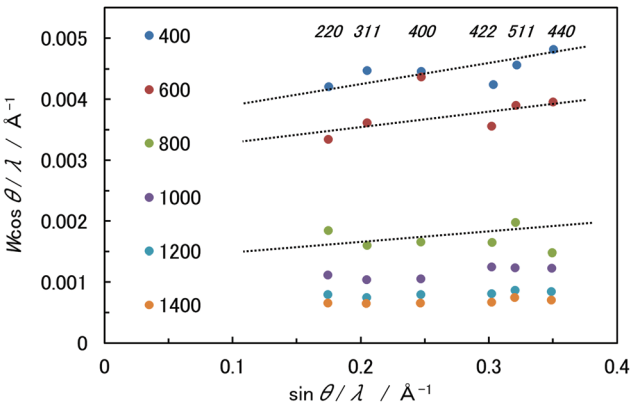

Fig. 4 Indexed Williamson–Hall plot of the products sintered at temperatures between 400 and 1400 °C.

Table 1 Lattice constant (a) calculated from XRD patterns. Crystallite sizes from XRD line broadening of the peaks

Products	Lattice constant a (Å)	Crystallite size (nm)
400	8.073(1)	20.2
600	8.087(1)	23.9
800	8.0953(5)	53.3
1000	8.1022(6)	78.3
1200	8.1089(4)	111
1400	8.1099(3)	132
JCPDS 82–2252	8.106	—
Ref. 13[a]	8.10735(1)	—
Ref. 13[a]	8.09853(1)	—
Ref. 14	8.1070(1)	—
Ref. 15	8.1078(3)	—
Ref. 16 (17)[b]	8.092	—
Ref. 18	8.10452(5)	—
Ref. 24[c]	8.0995	—
Ref. 24[c]	8.1051	—

[a] The top and bottom values are polycrystalline bulk and single crystal of $CoAl_2O_4$, respectively. [b] These references are from the same author and include the same value. [c] The top and bottom values are the values of the $CoAl_2O_4$ products synthesized at 800 and 1100 °C, respectively.

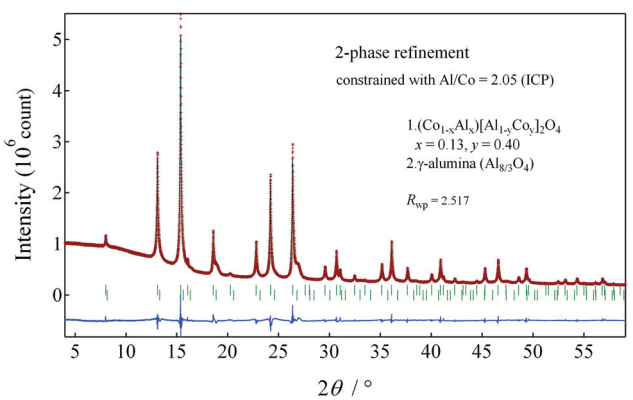

Fig. 5 SXRD pattern and Rietveld refinement for the **800** product. The measured intensities (red dots) are compared with the calculated profile using Rietveld refinement (black solid line). The Bragg positions of both the spinel structures, $(Co_{1-x}Al_x)[Al_{1-y}Co_y]_2O_4$ and γ-alumina, are indicated by the vertical green bars and the residual of the refinement is shown by the bottom blue solid line.

Table 2 Lattice constants, oxygen positional parameters, molar ratio, site occupancies, isotropic thermal factors, and Bragg reliability parameters for the respective phases of the **800** product. The weighted profile reliable parameter for the 2-phase refinement is R_{wp} = 2.517

Composition	a (Å)	x_O	Molar ratio	g	B_{iso} (Å^2)	R_B
Cobalt aluminate ($(Co_{0.87}Al_{0.13})[Al_{0.60}Co_{0.40}]_2O_4$)	8.09348(5)	0.26342(7)	0.56(1)	0.8710(37) (Co, 8a) 0.1290(4) (Al, 8a) 0.6000(31) (Al, 16d) 0.4000(26) (Co, 16d) 1 (Oxy)	 0.5 (8a) 0.5 (16d) 0.32 (Oxy)	4.317
γ-Alumina ($Al_{8/3}O_4$) (Ref. 35)	7.96669	0.2547(05)	0.44(1)	0.58 (Al, 8a) 0.84 (Al, 16d) 0.17 (Al, 32e) 1 (Oxy)	0.5 (8a) 0.5 (16d) 0.5 (32e) 0.5 (Oxy)	2.414

occupations at the T_d (A-) and O_h (B-) sites, respectively, showing non-stoichiometry of the cations and excess of Co ions. In the TG–DTA results, the weight loss of about 10% was seen in $Al(OH)_3$ and the precursor between 300 and 800 °C although there was no weight loss for $Co(OH)_2$ in the temperature range, suggesting that the Co content part in the precursor seems to decompose and/or melt more easily than the $Al(OH)_3$ part in it. It leads to some excess of Co in the final product at low temperature below 800 °C, suggesting the formation of a Co enriched spinel product. However, the product had a cation distribution in the structure, supporting the result of the Williamson–Hall plot. It suggests that the cation distribution seems to correlate with the lattice defects in the products. Additionally, from the viewpoint of the charge balance in the spinel structure of the **800** product, about 80% of Co^{3+} ions occupied the O_h site instead of Co^{2+} ions. It suggests that a large amount of Co^{3+} ions is contained in the products sintered at low temperatures, which is consistent with the TG–DTA results. Other previous work also points to the presence of Co^{3+} ions in samples prepared at low temperature.[19,20] The Co^{3+} ions seem to replace the Al^{3+} ions at the O_h site in the product. The evaluation of other products using the Rietveld refinement is in progress now. Note that the spinel cobalt aluminate products in this study are identified as $(Co_{1-x}Al_x)[Al_{1-y}Co_y]_2O_4$ ($x \neq y/2$).

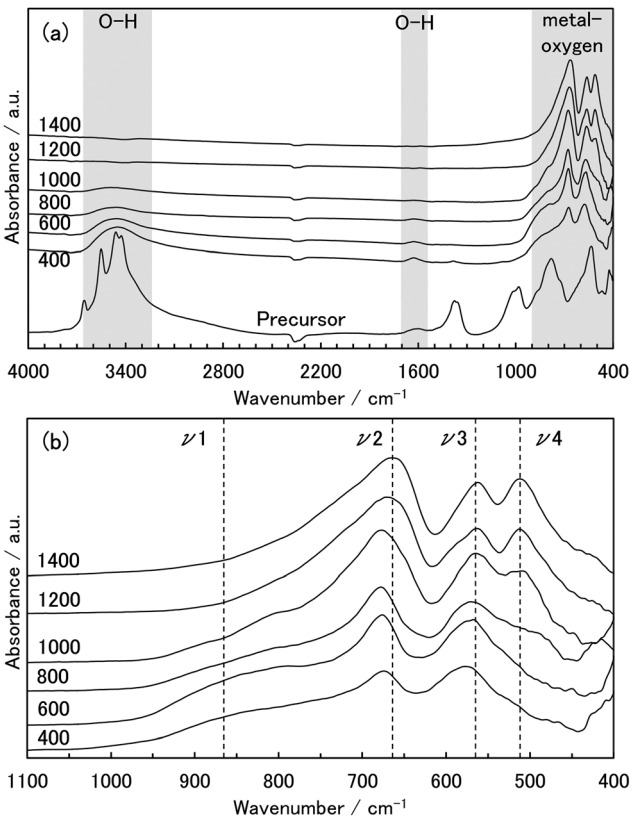

Fig. 6 (a) FT-IR spectra of the precursor and products sintered at the temperatures between 400 and 1400 °C. (b) Evolution of the spectra for the products enlarged in the range of 1100 to 400 cm^{-1}.

3. FT-IR spectroscopic analysis of the products

The FT-IR spectra of the products provide additional structural information (Fig. 6). The spectra of the products were very different from that of the precursor. The bands of the metal–oxygen bonds in spinel structure appear in the region between 1000 and 400 cm^{-1}.[20–23,37,42–44] In all of the products, distinctive bands around 670 (ν2) and 570 (ν3) cm^{-1} were observed (Fig. 6b). These two bands were similar to the bands observed for Co_3O_4.[37] A shoulder band is also present around 870 (ν1) cm^{-1} in the spectra from the **400–1000** products. The intensity of this shoulder decreases for the products sintered at higher temperatures. This trend is in contrast with the band around 510 cm^{-1} (ν4), which increases in intensity as the sintering temperatures rise above 800 °C. The observed three band structure (ν2, ν3, and ν4) in the FT-IR spectra is consistent with those previously reported for $CoAl_2O_4$.[20–23] Inspection of the product spectra reveals that the ν2 and ν3 bands shift to lower wavenumbers and the intensity of the ν2 band increases with increasing sintering temperature, suggesting a change in the bonding between the metal and oxygen ions in the spinel structure of the products ($(Co_{1-x}Al_x)[Al_{1-y}Co_y]_2O_4$). Considering some of the results from the XRD study, such as the sintering temperature variation on lattice constants and local distortion, observed changes in the FT-IR spectra may be the result of the strong dependence of the distribution of Co and Al ions on the sintering temperature.

Some distinctive bands were observed in the spectra of the products besides the metal–oxygen bands. A broad band between 3600 and 3200 cm^{-1} and a band at around 1650 cm^{-1} were seen in the spectra for the **400–1000** products. These

bands were attributed to the O–H mode of chemisorbed water and/or terminated hydroxides,[25–27,45,46] suggesting that water and/or hydroxide groups are chemisorbed on the surface and/or incorporated into the product crystals.[46] Chemisorbed water and/or terminated hydroxides are believed to coordinate to the metal ions and possibly cause lattice defects in the products.[26–28] The O–H bands disappear in the spectra of the products prepared at high temperatures above 1200 °C, which is particularly noticeable in the bands between 3600 and 3200 cm^{-1}. The weakened intensity of these bands indicates a decrease in the amount of the chemisorbed water and/or the terminated hydroxides. From the Williamson–Hall plot of the products (Fig. 4), the degree of the lattice defects in the **400–800** products was higher than that in the **1000–1400** products. The amount of chemisorption, therefore, seems to correlate to the quantity of lattice defects in the products. Notably, the chemisorption seems to strongly affect the crystallinity of the products with small crystallite size since the surface-to-volume ratio is generally large for nanosized crystals. Although the chemisorption was detected in the **1000** product, the degree of lattice defects was the same as those of the **1200** and **1400** products. The chemisorption possibly does not affect the crystallinity of the **1000** product.

4. UV–VIS spectroscopic analysis of the products

The color of the spinel structure products varied with the sintering temperature (Fig. S1†). As mentioned previously, the **1000–1400** products had a blue color, while the color of the low-temperature **400–800** products was dark green. The product color comes from the Co ion because pure aluminum oxides and hydroxides show little absorption in the visible region. No distinctive absorption bands were observed in the region for the spectra of $Al(OH)_3$ and Al_2O_3 (not shown). The color change of the products suggests a change in the crystal (ligand) field, such as the coordination environment and/or a valence change of the Co ion.[47,48] The absorption spectrum for the Co ion is known to contain contributions from a spin-allowed, d–d transition with Jahn–Teller distortion of the coordination structure and ligand-to-metal charge transfer (LMCT).[47,48]

The UV–VIS spectrum of the precursor shows bands around 530 and 450 nm, which are assigned to the d–d transition of the Co^{2+} ion with the octahedral (O_h) structure of Co–AlHtc in the precursor (Fig. 7).[36,47,48] These transition bands are from the $^4T_{1g}$ ground state of the d^7 electrons.[47,48] The spectra of the **1000–1400** products are similar to the well-studied spectrum of the $CoAl_2O_4$ blue pigment.[19–24] The pronounced bands around 620, 580, and 550 nm were assigned to the $[^4A_2(F) \rightarrow {}^4T_1(P)]$ of the d–d transitions of the Co^{2+} ion at the T_d site.[19–24,47,48] The distinctive blue color originates from these absorption bands, which are increasingly prominent for the products formed under a higher sintering temperature, suggesting that the amount of Co^{2+} ion at the T_d site increases in the spinel structure. In the **1200** and **1400** products, small bands around 480 and 410 nm appeared in the spectra and were assigned to the spin-forbidden d–d transition of the Co^{2+} ion at the T_d site.[20,48]

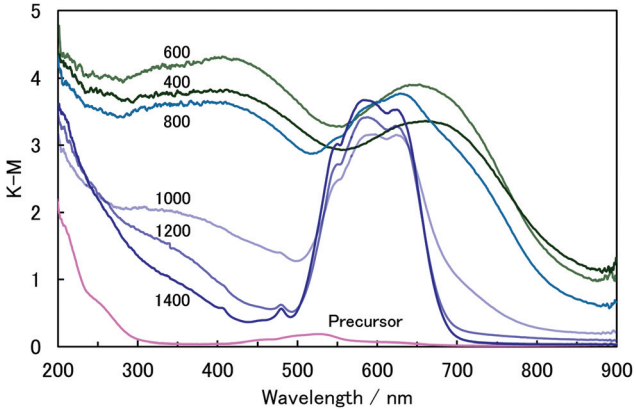

Fig. 7 UV–VIS powder diffuse reflectance spectra of the precursor and the products sintered at the temperatures between 400 and 1400 °C.

In contrast, the spectra for the **400–800** products were noticeably different from those of the **1000–1400** products. The spectra of the **400** and **600** products, with a dark green color, show two broad absorption bands, one between 800 and 550 nm and the other between 550 and 300 nm. These spectra were similar to that of Co_3O_4,[38,49] and according to the band assignment for Co_3O_4, the two aforementioned bands were assigned as LMCT bands. The band between 800 and 550 nm arises from LMCT from O^{2-} to Co^{3+} ions at the O_h site, and the band between 550 and 300 nm is from LMCT from O^{2-} to Co^{2+} ions at the T_d site in the products with spinel structures ($(Co_{1-x}Al_x)[Al_{1-y}Co_y]_2O_4$), respectively. The color of the **800** product was dark aqua, and there was a broad band between 550 and 300 nm in the spectrum. However, the broad band between 800 and 550 nm split into several bands around 620, 580, and 550 nm, representing the d–d transitions of the Co^{2+} ion at the T_d site. Additionally, a broad band around 720 nm was observed and assigned as a LMCT band from O^{2-} to Co^{3+} ions at the O_h site. Note that the band between 550 and 300 nm and the band around 720 nm decreases in the spectra of the **1000–1400** products. The band below 400 nm remains a shoulder, and therefore can be assigned to the LMCT band from O^{2-} to Co^{2+} ions at the T_d site in $CoAl_2O_4$ with blue color. These optical results are consistent with the TG–DTA and XRD analyses showing the presence of the Co^{3+} ion. The drastic change in the spectra between the **800** and **1000** products may be attributed to the reduction of the Co^{3+} and a characteristic configuration of the cations in the metallic sites of the spinel structure. However, since the shoulder band around 720 nm was seen in the spectrum of the **1000** product, the reduction from Co^{3+} to Co^{2+} ions does not seem to finish at 1000 °C for 2 hours. In other words, almost all of the Co ions come to reside on the T_d (A-) site as Co^{2+}.

The blueness (b^* value) of the products increased with increasing sintering temperature (Table 3). Notably, the blueness of the **1200** and **1400** products was remarkably high compared to measurements reported previously.[24,31,50] This simple and rapid synthesis method for preparing spinel cobalt aluminate products with a bright blue color could thus be useful for the synthesis of industrial pigment.

Table 3 CIE $L^*a^*b^*$ colorimetric parameters of the precursor, the products sintered at the temperatures between 400 and 1400 °C, and values reported in the literature

Products	L^*	a^*	b^*
Precursor	83.3	9.91	−2.59
400	41.8	−1.95	4.04
600	40	−2.74	3.92
800	41.2	−4.32	1.21
1000	47.2	−7.74	−9.57
1200	50.3	−6.47	−26
1400	49.9	−0.13	−35.4
Ref. 24[a]	32	—	−16
Ref. 24[a]	26	—	−26
Ref. 31	81.99	−3.9	−15.62
Ref. 50	38.63	−3.28	−14.39

[a] The top and bottom values are the values of the $CoAl_2O_4$ products synthesized at 800 and 1100 °C, respectively.

5. Magnetic analysis of the products

According to the structural and optical analyses described above, the coordination environment and the electronic state of the Co ions in the spinel structure ($(Co_{1-x}Al_x)[Al_{1-y}Co_y]_2O_4$) strongly depend on the sintering temperature. These variations can be further verified by magnetic analysis since changes in the coordination environment of the Co ions affect the magnetic moment. Theoretical calculations have shown that the magnetic state of a Co^{2+} ion located on the T_d or O_h site is distinguishable because the number of unpaired d-electrons on the Co^{2+} ion is different.[16] Additionally, the valence change of the Co ions can also affect the magnetic moment.

Temperature, T, dependencies of the molar magnetic susceptibilities, χ, and inverse susceptibilities, χ^{-1}, for the products were investigated (Fig. 8). Both the χ–T and χ^{-1}–T curves of the products changed systematically. In the low temperature region, the χ–T curves of the **400**–**1000** products were quite different from those of the **1200** and **1400** products (Fig. 8a). A magnetic anomaly around 10 K was observed for the **1200** and **1400** products and is similar to what was seen in previous studies.[11–15] In the **400**–**1000** products, the behavior of the χ–T curves is similar, and the magnetic transition is indistinguishable. The χ^{-1}–T curves of all the products followed the Curie–Weiss (CW) law in the higher temperature regions (Fig. 8b). It should be noted that, even though the Co^{3+} ion was contained in the **400**–**1000** products, the magnetic behaviors were quite different from that of Co_3O_4 that shows an antiferromagnetic transition at 33 K.[14,30,38,51] The magnetic behavior of Co_3O_4 prepared from the reference $Co(OH)_2$ was thus different from that of all the products (Fig. S2†). As expected, the prepared Co_3O_4 products showed an antiferromagnetic transition around 30 K. The difference in the magnetic properties between the products and Co_3O_4 also proves that the spectral data obtained for the products contained no Co_3O_4 impurities. Tristan *et al*. synthesized spinel $Co[Al_{1-x}Co_x]_2O_4$ ($x > 0$), and the magnetic properties of them were measured.[14] The maximum point in the susceptibility increases with increasing x in $Co[Al_{1-x}Co_x]_2O_4$, that is, the antiferromagnetic behavior is

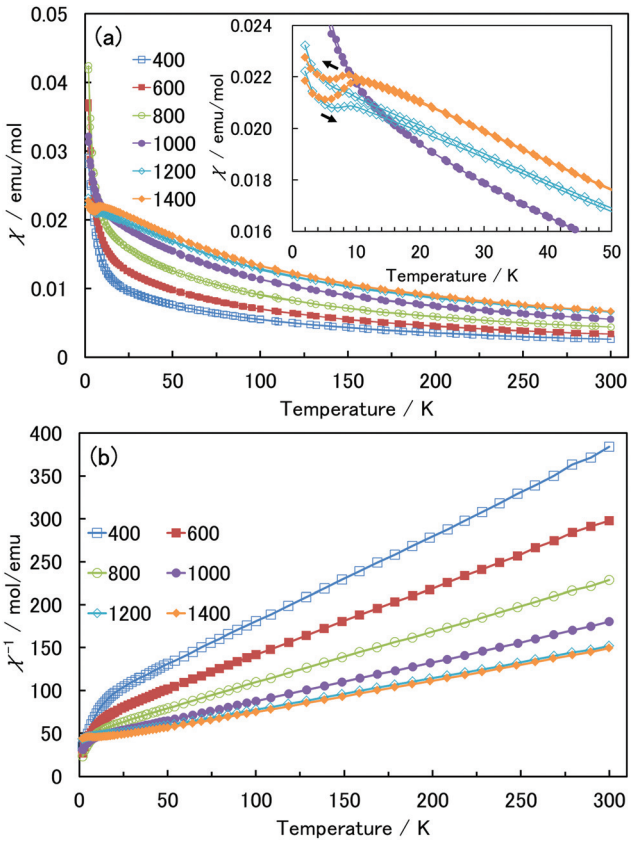

Fig. 8 (a) Zero-field-cooled and field-cooled magnetic susceptibility (χ) *versus* temperature (T) plots measured at 100 Oe. The inset shows enlarged χ–T plots. (b) Inverse susceptibility (χ^{-1}) *versus* temperature (T) plots of the products sintered at temperatures between 400 and 1400 °C.

stabilized with increasing x. The magnetic susceptibilities of $Co[Al_{1-x}Co_x]_2O_4$ with various x values are different from those of our products sintered at low temperatures in this study. Therefore, the magnetic behaviors of the products sintered at low temperatures seem to be an intrinsic phenomenon, although the products are nonstoichiometric. It suggests that undiscovered spinel products were formed at low temperatures that is possibly induced by various cation distributions in the spinel structure ($(Co_{1-x}Al_x)[Al_{1-y}Co_y]_2O_4$).

The Weiss temperature (θ), the Curie constant (C), and the effective moment (p_{eff}) for all products were calculated (Table 4). The values of p_{eff} for the **1200** and **1400** products were close to the values for high-temperature synthesized $CoAl_2O_4$,[11–15] suggesting that both the magnetic moment and magnetic interactions systematically decreased by lowering the sintering temperature. Unpaired d-electrons of the Co^{2+} ions decreased through changing the coordination environment of the Co^{2+} ions from the T_d to the O_h sites and the formation of Co^{3+} ions at the O_h sites in the spinel structure. The $p_{eff\text{-}cal}$ of the **800** product, $3.45\mu_B$, was estimated from the result of the Rietveld refinement, $(Co_{0.87}Al_{0.13})[Al_{0.60}Co_{0.40}]_2O_4$ and $n = 0.56$. Remarkably, as indicated in Table 4, the $p_{eff\text{-}cal}$ is close to the observed p_{eff} for the **800** product. Note that the mixed valent

Table 4 Curie constants (C), Weiss temperature (θ), and effective moment (p_{eff}) determined from the CW fits to the magnetic susceptibility of the products and the inversion parameter, α, estimated from the magnetic quantities

Products	Curie constant: C (emuK mol^{-1})	Curie–Weiss temperature : θ (K)	Effective moment: p_{eff} (μ_B)
400	1	−79.9	2.83
600	1.27	−80.2	3.19
800	1.68	−83.6	3.67
1000	2.18	−90.7	4.18
1200	2.7	−109	4.65
1400	2.71	−102	4.66
Ref. 11	—	−96(8)	4.46(5)
Ref. 12	—	−89(6)	4.45(8)
Ref. 13[a]	—	−99(1)	4.62(2)
Ref. 13[a]	—	−94(1)	4.63(2)
Ref. 14	—	−119	4.88
Ref. 15	—	−104(2)	4.65(9)
$Np_{eff\text{-}theo}$[b]	—	—	4.65

[a] The top and bottom values are polycrystalline bulk and single crystal of $CoAl_2O_4$, respectively. [b] The theoretical effective moment ($Np_{eff\text{-}theo}$) of the normal spinel structure was shown.

state of the Co ion at the O_h site is expected to establish due to the charge neutrality in the determined crystallographic state, that is, 16% Co^{2+} and 84% Co^{3+} ions at the O_h site. As shown in Fig. S3,† broadening of the ^{27}Al-NMR spectra can be attributed to changes in the internal magnetic field resulting from the magnetic spin on the Co^{2+} ions around the Al ions,[21] most likely *via* the dipole–dipole or the transferred hyperfine interactions. These magnetic properties are also consistent with the structural and optical analyses, and are reflected by the cation distribution. The spectra of the **400** and **800** products can be assigned to γ-Al_2O_3 as the impurity phase. It should be emphasized that besides the sharp signal weak broad signals were seen in the spectra which can be assigned to ^{27}Al nuclei surrounded by the electronic spins on Co ions dominating in the cation sites of the spinel structure. Note that the sharp component in the spectrum is apparently intensified compared with the broad component, since the excitation frequency region and power are limited in this ^{27}Al-NMR measurement.

The experimental data show the presence of lattice distortions and/or Al_2O_3 as impurities in the products, and the non-stoichiometry of the cations. The changes in the crystallographic and the physical properties are not only attributed to the changes in the valence state of the Co ions but also to the cation distributions in the spinel structure ($(Co_{1-x}Al_x)[Al_{1-y}Co_y]_2O_4$). The physical properties of the products sintered at low temperatures were undiscovered. Since the physical properties of the products sintered at high temperatures were similar to that of conventional spinel $CoAl_2O_4$, the stoichiometry of them seems to be close to the conventional one. These results suggest that the cation distribution strongly affects the physical properties. These unique properties contribute to the crystallographic degree of freedom in the spinel-type $CoAl_2O_4$.

Conclusion

A simple and rapid method for the synthesis of spinel cobalt aluminate products ($(Co_{1-x}Al_x)[Al_{1-y}Co_y]_2O_4$ with $x \neq y/2$) *via* sintering of a hydroxide precursor was developed and described. Products prepared at temperatures over 1000 °C were essentially the commonly described form of $CoAl_2O_4$ known as blue pigment. Interestingly, however, low temperature preparation (>400 °C) of the products with a spinel structure as the main phase was also achieved. Lattice constants and crystallite sizes of the products systematically increased with increasing sintering temperature. The color of the products turned from dark green at low temperatures to blue between 800 and 1000 °C. The products prepared at temperatures over 1000 °C were bright blue. This blue color was attributed to the d–d transition of the Co^{2+} ion at the T_d site in the spinel structure. Therefore, the degradation of the blue color in the low-temperature formation of the products resulted from the decrease of the Co^{2+} ion at the T_d site. The degree of lattice defects in the products prepared at temperatures below 1000 °C tended to be high compared to the high-temperature products. The low-temperature products also showed evidence of chemisorbed water and/or hydroxide groups. These results are possibly due to the reduction of the Co^{2+} ion at the T_d site and subsequent increase of the amount of Co^{3+} ion at the O_h site. The Weiss temperature and the effective moment of the products increased with increasing sintering temperature. The magnetic analysis suggested that an extreme change in the cation distribution occurred for the low-temperature products. The products from the low-temperature preparation showed a change in both the valence of the Co ions and the cation distribution in the spinel structure.

The described preparation technique for synthesizing spinel cobalt aluminate products is simpler and faster than the conventional solid-phase reaction and can thus have direct industrial application. This study revealed that the physical properties of the products prepared at low temperature were very different from that of conventional $CoAl_2O_4$ known as blue pigment. The obtained properties are also important for the development of novel functional materials for $CoAl_2O_4$. Treatment at low temperature seems to be important for controlling the cation distribution of spinel $CoAl_2O_4$. While this low-temperature sintering method using a hydroxide precursor is very effective for the preparation of spinel cobalt aluminate products, the presence of Co^{3+} ions and Al_2O_3 should be eliminated as much as possible, and the stoichiometry of the cations in the spinel products should be the same as that of conventional $CoAl_2O_4$ and will be the next issue of this study.

Acknowledgements

This work was partially supported by Grant-in-Aids for Scientific Research (KAKENHI) (A) No. 21241023 and (S) No. 20226015.

References

1 I. B. Bersuker, *Electronic Structure and Properties of Transition Metal Compounds*, John Wiley & Sons, New York, 1996.
2 E. P. Wohlfarth, *Ferromagnetic Materials: a handbook on the properties of magnetically ordered substances vol. 3*, Elsevier, New York, 1982.
3 P. A. Cox, *Transition Metal Oxides*, Oxford University, New York, 1992.
4 E. B. Faulkner and R. J. Schwartz, *High Performance Pigments*, Wiley-VCH, Weinheim, 2009.
5 G. Buxbaum and G. Pfaff, *Industrial Inorganic Pigments*, Wiley-VCH, Weinheim, 2005.
6 L. D. Kock and D. De Waal, *J. Raman Spectrosc.*, 2007, **38**, 1480–1487.
7 L. Ji, S. Tang, H. C. Zeng, J. Lin and K. L. Tan, *Appl. Catal. A*, 2007, **207**, 247–255.
8 A. Walsh, Y. Yan, M. M. Al-Jassim and S.-H. Wei, *J. Phys. Chem. C*, 2008, **112**, 12044–12050.
9 A. Walsh, S.-H. Wei, Y. Yan, M. M. Al-Jassim and J. A. Turner, *Phys. Rev. B: Condens. Matter*, 2007, **76**, 165119/1–165119/9.
10 K.-S. Ahn, Y. Yan, M.-S. Kang, J.-Y. Kim, S. Shet, H. Wang, J. Turner and M. M. Al-Jassim, *Appl. Phys. Lett.*, 2009, **95**, 022116/1–022116/3.
11 M. Hagiwara, S. Kimura, N. Nishihagi, T. Suzuki, M. Nohara, H. Takagi and K. Kindo, *J. Low Temp. Phys.*, 2010, **159**, 11–14.
12 T. Suzuki, H. Nagai, M. Nohara and H. Takagi, *J. Phys.: Condens. Matter.*, 2007, **19**, 145265/1–145265/5.
13 A. Maljuk, V. Tsurkan, O. Zeharko, A. Cervellino, A. Loidl and D. N. Argyriou, *J. Cryst. Growth*, 2009, **311**, 3997–4000.
14 N. Tristan, V. Zestrea, G. Behr, R. Klingeler, B. Büchner, H. A. Krug von Nidda, A. Loidl and V. Tsurkan, *Phys. Rev. B: Condens. Matter*, 2008, **77**, 094412/1–094412/10.
15 N. Tristan, J. Hemberger, A. Krimmel, H. A. Krug von Nidda, V. Tsurkan and A. Loidl, *Phys. Rev. B: Condens. Matter*, 2005, **72**, 174404/1–174404/9.
16 F. Tielens, M. Calatayud, R. Franco, J. M. Recio, J. Pérez-Ramírez and C. Minot, *J. Phys. Chem. B*, 2006, **110**, 988–995.
17 F. Tielens, M. Calatayud, R. Franco, J. M. Recio, J. Pérez-Ramírez and C. Minot, *Solid State Ionics*, 2009, **180**, 1011–1016.
18 A. Nakatsuka, Y. Ikeda, Y. Yamasaki, N. Nakayama and T. Mizota, *Solid State Commun.*, 2003, **128**, 85–90.
19 N. El Habra, L. Crociani, C. Sada, P. Zanella, M. Casarin, G. Rossetto, G. Carta and G. Paolucci, *Chem. Mater.*, 2007, **19**, 3381–3386.
20 M. Zayat and D. Levy, *Chem. Mater.*, 2000, **12**, 2763–2769.
21 F. Mayer, R. Hempelmann, S. Mathur and M. Veith, *J. Mater. Chem.*, 1999, **9**, 1755–1763.
22 U. Lavrenčič Štangar, B. Orel and M. Krajnc, *J. Sol-Gel Sci. Technol.*, 2003, **26**, 771–775.
23 M. Salavati-Niasari, M. Farhadi-Khouzani and F. Davar, *J. Sol-Gel Sci. Technol.*, 2009, **52**, 321–327.
24 M. Gaudon, A. Apheceixborde, M. Ménétrier, A. Le Nestour and A. Demourgues, *Inorg. Chem.*, 2009, **48**, 9085–9091.
25 M. Taguchi, S. Takami, T. Adschiri, T. Nakane and T. Naka, *CrystEngComm*, 2012, **14**, 2132–2138.
26 M. Taguchi, S. Takami, T. Adschiri, T. Nakane and T. Naka, *CrystEngComm*, 2012, **14**, 2117–2123.
27 M. Taguchi, S. Takami, T. Adschiri, T. Nakane and T. Naka, *CrystEngComm*, 2011, **13**, 2841–2848.
28 J. Zhang, T. Naka, S. Ohara, K. Kaneko, T. Trevethan, A. Shluger and T. Adschiri, *Phys. Rev. B: Condens. Matter*, 2011, **84**, 045411/1–045411/9.
29 M. Taguchi, S. Takami, T. Naka and T. Adschiri, *Cryst. Growth Des.*, 2009, **9**, 5297–5303.
30 T. Mousavand, T. Naka, K. Sato, S. Ohara, M. Umetsu, S. Takami, T. Nakane, A. Matsushita and T. Adschiri, *Phys. Rev. B: Condens. Matter*, 2009, **79**, 144411/1–144411/5.
31 D. Rangappa, T. Naka, A. Kondo, M. Ishii, T. Kobayashi and T. Adschiri, *J. Am. Chem. Soc.*, 2007, **129**, 11061–11066.
32 K. Sato and T. Naka, *et al.*, *J. Magn. Magn. Mater.*, submitted.
33 H. Miura, *J. Crystallogr. Soc. Jpn.*, 2003, **45**, 145–147.
34 G. K. Williamson and W. H. Hall, *Acta Metall. Mater.*, 1953, **1**, 22–31.
35 R.-S. Zhou and R. L. Synder, *Acta Crystallogr., Sect. B: Struct. Sci.*, 1991, **45**, 617–630.
36 J. Pérez-Ramírez, G. Mul, F. Kapteijn and J. A. Moulijn, *J. Mater. Chem.*, 2001, **11**, 821–830.
37 Z. P. Xu and H. C. Zeng, *J. Mater. Chem.*, 1998, **8**, 2499–2506.
38 S. Thota, A. Kumar and J. Kumar, *Mater. Sci. Eng., B*, 2009, **164**, 30–37.
39 *International Chemical Safety Cards* # 0373 Aluminum Hydroxide ($Al(OH)_3$).
40 S. Cava, S. M. Tebcherani, S. A. Pianaro, C. A. Paskocimas, E. Longo and J. A. Varela, *Mater. Chem. Phys.*, 2006, **97**, 102–108.
41 S. Tsunekawa, J.-T. Wang and Y. Kawazoe, *J. Alloys Compd.*, 2006, **408–412**, 1145–1148.
42 H. D. Lutz, B. Müller and H. J. Steiner, *J. Solid State Chem.*, 1991, **90**, 54–60.
43 P. C. Garcia and I. Rasines, *J. Solid State Chem.*, 1984, **52**, 187–193.
44 N. W. Grimes and A. J. Collett, *Phys. Status Solidi B*, 1971, **43**, 591–599.
45 K. Nakanishi, *Infrared Absorption Spectroscopy: Practical*, Holden-Day, San Francisco, 1962.
46 K. Nakamoto, *Infrared and Raman Spectra of Inorganic and Coordination Compounds*, Wiley, New York, 1997.
47 D. Sutton, *Electronic Spectraof Transition Metal Complexes*, McGraw-Hill, New York, 1968.
48 C. J. Ballhausen, *Introduction to Ligand Field Theory*, McGraw-Hill, New York, 1962.
49 M. Lenglet and C. K. Jørgensen, *Chem. Phys. Lett.*, 1994, **229**, 616–620.
50 L. K. C. de Souza, J. R. Zamian, D. N. da Rocha Filho, L. E. B. Soledade, I. M. G. dos Santos, A. G. Souza, T. Scheller, R. S. Angélica and C. E. S. da Costa, *Dyes Pigm.*, 2009, **81**, 187–192.
51 W. L. Roth, *J. Phys. Chem. Solids*, 1964, **25**, 1–10.